Ultrasensitive prostate cancer marker PCA3 detection with impedimetric biosensor based on specific label-free aptamers

TAKITA, Sarra <http://orcid.org/0000-0002-1376-0135>, NABOK, Aleksey <http://orcid.org/0000-0002-9078-1757>, MUSSA, Magdi, KITCHEN, Matthew, LISHCHUK, Anna and SMITH, David <http://orcid.org/0000-0001-5177-8574>

Biosensors and Bioelectronics: X 18 (2024) 100462

Contents lists available at ScienceDirect

Biosensors and Bioelectronics: X

journal homepage: www.journals.elsevier.com/biosensors-and-bioelectronics-x

Ultrasensitive prostate cancer marker PCA3 detection with impedimetric biosensor based on specific label-free aptamers

Sarra Takita [a,c,*], Alexi Nabok [a], Magdi Mussa [a,d], Matthew Kitchen [a], Anna Lishchuk [a,b], David Smith [c]

[a] Sheffield Hallam University, Materials and Engineering Research Institute, City Campus, Howard Street, Sheffield, S1 1WB, UK
[b] The University of Sheffield, Department of Chemical and Biological Engineering, Mappin St., Sheffield City Centre, Sheffield, S1 4LZ, UK
[c] Sheffield Hallam University, Biomolecular Sciences Research Centre, City Campus, Howard Street, Sheffield, S1 1WB, UK
[d] The Institute of Marine Engineering, Science and Technology, London, SW1H 9JJ, UK

ARTICLE INFO

Keywords:
Prostate cancer
PCA3
Aptamer
Screen-printed electrodes
Electrochemical impedance spectroscopy (EIS)
Cancer diagnostics

ABSTRACT

Prostate cancer (PCa) appears among the most frequently diagnosed types of malignancies in males. Because of the high demand and increasing detection rate of early PCa, alongside the specificity limitations of the gold standard clinical tools available for the diagnosis and prognosis of prostate cancer, there is an urgent need for more reliable PCa markers and highly sensitive diagnostic tools to avoid under-treatment and over-diagnosis. PCA3, or prostate cancer antigen 3, is a potential prostate cancer biomarker that is more specific and useful for preventing unnecessary repeat biopsies, particularly in men with persistently high prostate-specific antigen indices after a negative biopsy. Additionally, an electrochemically based biosensor would prove to be a powerful diagnostic tool for PCA3 detection in urine because of its simplicity, sensitivity, and cost-effectiveness, in contrast to the more traditional PCa diagnostics that depend on blood testing. This paper aimed to design a novel and simple electrochemical impedimetric biosensor based on a label-free RNA-aptamer (CG3-PCA3) as the molecular recognition element for detecting PCA3. The proposed aptasensor for the detection of PCA3 has been developed using a screen-printed carbon electrode (SPCE) modified by gold nanoparticles (AuNPs), further improving sensitivity and allowing the immobilisation of thiolate aptamers on its surface. The findings presented here demonstrated a high sensitivity to PCA3, with a detection limit of 20 fM in artificial urine and 1 fM in buffer. These results indicate that the PCA3 aptasensor could be a promising tool for routine PCa diagnosis due to its high sensitivity and cost-effectiveness.

1. 1- Introduction

Cancer remains the leading cause of mortality despite current advances in medical treatment. Therefore, early detection of the disease before it spreads to other organs is essential for effective cancer therapy and saving patients' lives. A particular case that has a worldwide effect is prostate cancer (PCa); it is the fifth most common cause of life-threatening cancer and the second most commonly diagnosed cancer among men (Sung et al., 2021). In most countries, the incidence rate for PCa has increased above 20% over the past decade (Sung et al., 2021). Because of its asymptomatic development, PCa is incurable if detected in its later stages and a silent threat in its early stages (Sung et al., 2021; Velonas et al., 2013). Thus, early diagnosis is a key element in its management (Kupelian et al., 2006; U.S National Cancer Institute, 2017). This led to the introduction of tumour biomarkers, which are chemical substances that indicate the existence of cancerous tissues at levels far higher than those seen in healthy tissues (Li et al., 2020; Ludwig and Weinstein, 2005). These biomarkers can be found in tissue and body fluids such as urine and blood, which could be used for the early detection of certain diseases (Ludwig and Weinstein, 2005). Prostate-specific antigen (PSA) is currently the most commonly used biomarker in blood to detect and monitor patients with PCa, combined with other prostate assessments such as biopsies, magnetic resonance imaging, and digital rectal examination (DRE); A physician inserts a gloved finger into the rectum to inspect for any swelling or bumps of the prostate gland (Jolly et al., 2015; Mitchell et al., 2008). However, the PSA test has low clinical specificity as PSA appears to be an organ-specific biomarker rather than a cancer-specific biomarker

* Corresponding author. Sheffield Hallam University, Materials and Engineering Research Institute, City Campus, Howard Street, Sheffield, S1 1WB, UK.
E-mail address: S.Takita@shu.ac.uk (S. Takita).

https://doi.org/10.1016/j.biosx.2024.100462
Received 25 December 2023; Received in revised form 7 March 2024; Accepted 10 March 2024
Available online 16 March 2024

(Center et al., 2012). It also often produces false-positive results for a variety of benign diseases. Even worse, false-negative PSA test results relate to certain uncommon situations in which tumours may develop even before high PSA concentrations are detected (Lomas and Ahmed, 2020). As a result of the drawbacks of the current PSA test, unnecessary biopsies and excessive treatment of indolent cancers occur, which notably reduces the quality of life without improving survival rates (Adhyam and Gupta, 2012; Lomas and Ahmed, 2020; Macefield et al., 2010). Thus, finding prostate cancer-specific markers is crucial for improving the accuracy of PCA diagnostics, minimising biopsy procedures, and identifying patients with potentially life-threatening PCa. Ultimately, this will also help categorise patients based on disease aggressiveness and increase the chances of implementing effective medical interventions (Moyer, 2012). Prostate Cancer Antigen 3 (PCA3) can potentially be useful in developing more reliable diagnostic techniques for PCa. PCA3 can potentially be useful in developing more reliable diagnostic techniques for prostate cancer (PCa). PCA3 is classified as a long noncoding RNA (lncRNA), meaning it does not participate in protein synthesis. It is highly expressed in prostate tumour cells and malignant tissues, with a 34-fold increase compared to its normal expression in healthy tissues. This elevated expression in PCA3 can differentiate between aggressive and non-aggressive forms of the disease (Hessels and Schalken, 2009; De Kok et al., 2002; Ploussard and de la Taille, 2018). Unlike PSA serum levels, PCA3 expression has been shown to have a better specificity in predicting the results of prostatic biopsies, particularly when used with other predictive markers like PSA (Bourdoumis et al., 2010; Wu et al., 2012). Above all that, urine-based diagnostics are preferred because of their physical proximity to the prostate, low amounts of urinary protein, and the potential for genuinely non-invasive repeated sampling. The US Food and Drug Administration (FDA) has approved PCA3 as a urine marker for diagnosing prostate cancer (PROGENSA's quantitative PCA3 test); the test is currently adopted in 72 laboratories across the world (Bernardeau et al., 2017; Groskopf et al., 2006; Sartori and Chan, 2014). The method relies on using Gen-Probe Incorporated's specific target capture, detection with chemiluminescent DNA probes and transcription-mediated amplification (TMA). The score is determined by normalising PCA3 expression with PSA expression, which serves as a housekeeping gene for prostate tissue. A correlation indicates a connection between the PCA3 score and the probability of a positive biopsy (Bernardeau et al., 2017; Liss et al., 2011), leading to reducing unnecessary biopsies procedures. Additionally, the method is beneficial in identifying individuals with elevated PSA levels due to nonspecific causes. These findings encouraged further investigation and development of PCA3 detection methods (Groskopf et al., 2006; Kanyong et al., 2016; TINZL et al., 2004). Despite the FDA's approval and high sensitivity, these methods still have some drawbacks. These include time of analysis, cost (especially for a point-of-care device), and complicated workflow; there is no simple procedure for PCA3 detection. Additionally, they require highly specialised laboratories, which is likely the primary reason why PCA3 tests cannot be feasibly used for routine clinical purposes. Obviously, there is a clear need to create simple, sensitive, and cost-effective procedures with the potential for rapid point-of-care diagnostic technology. The progress in this field is being achieved by the adoption of electrochemical (EC)-based biosensors, having several benefits in terms of sensitivity, cost-effectiveness, the ability to be integrated with point-of-care devices, and speed of response (Drobysh et al., 2022a; Forouzanfar et al., 2020; Jolly et al., 2015). In addition, the EC aptasensor, which uses an aptamer as the biological recognition element, was chosen and applied in the present study because it is a relatively promising alternative for clinical implementation (Das and Kelley, 2020; Forouzanfar et al., 2020). Aptamers (APTs) are artificially selected short single-stranded DNA or RNA oligonucleotides and possess a high level of selectivity, like enzymes or antibodies, in their ability to bind to specific target molecules. Additionally, aptamers exhibit better thermal and environmental stability (Pfeiffer and Mayer, 2016; Toh et al., 2015). In recent years, scientists have been interested in label-free electrochemical apta-sensors due to their label-free, cost-effective, fast detection speed and simple operation (Rizwan et al., 2018). The main detection used in such sensors is electrochemical impedance spectroscopy (EIS), which records an electrochemical system's responses (current and phase) as a function of frequency to an applied oscillating potential. The EIS method is a non-destructive, sensitive, and cost-efficient technique; the target molecules can be directly detected through measured impedance changes of the sensing layer in response to a small amplitude perturbation without the need for any external modification of the biomolecules (Karapetis et al., 2018) for investigating the properties of surface-modified electrodes (Montagut et al., 2020), as well as other applications like measuring barrier of coating and corrosion (Mussa et al., 2021, 2023). Besides, the use of commercial screen-printed electrodes (SPEs) in electrochemical biosensing and apta-sensing is widespread these days; a useful analytical tool that can meet the demands of cost-effective, miniaturisation and reduction of analyte volume in bioassay applications for early point-of-care diagnostics (Drobysh et al., 2022b, 2024; Wang et al., 2019). Recently, several types of biosensors for PCA3 detection based on different sensing principles, using different substrate materials (gold, carbon, nano-structured materials), different bio-receptors (labelled and non-labelled DNA- and RNA-based aptamers and DNA-probes) and different analytical methods have been demonstrated. For example, electrochemical sensors for PCA3 utilising redox-labelled aptamers were demonstrated in (Nabok et al., 2021; Takita et al., 2023). Optical biosensors utilising the method of total internal reflection ellipsometry in conjunction with the use of label-free aptamer showed equally high sensitivity and also allowed the evaluation of the aptamer affinity towards the PCA3 target (Takita et al., 2021). Biosensors based on surface-enhanced Raman scattering (SERS) (Fu et al., 2019) and electrochemical genosensors (Rodrigues et al., 2021; Soares et al., 2019) also showed high sensitivity to PCA3 detection in femtoMole range. Despite significant advancements in PCA3 detection techniques and numerous attempts to introduce simple and easy-to-use biosensors for monitoring PCA3, achieving high sensitivity for PCA3 detection remains challenging. Furthermore, high analytical costs, insufficient portability for point-of-care applications, and the need for specialised equipment as well as personnel are some of the downsides of these detection approaches (Shayesteh and Ghavami, 2020). Moreover, to the best of our knowledge, few attempts have been made among these sensors to investigate the PCA3 by applying an aptamer-based EIS detection approach. To improve the performance of the aptamer-based biosensor, a combination of non-labelled aptamers with nano-structured materials has been used in this work. According to several studies, the use of gold nanoparticles (AuNPs) as a platform for the development of electrochemical apta-sensors is beneficial due to their unique properties, such as simplicity in functionalization with aptamers, good conductivity, high specific surface area, and low toxicity (Adabi et al., 2021; Fang et al., 2017). AuNPs can be easily deposited on low-cost screen-printed carbon electrodes, which is important for mass manufacturing (Pasinszki et al., 2017). Therefore, in response to the need for improved sensitivity and specificity for PCA3 diagnosis, a simple, cost-effective approach is potentially suitable for point-of-care applications. In this work, we used commercially available screen-printed carbon electrodes (SPCE) that were coated with gold nanoparticles (AuNPs) as a substrate for immobilising an aptamer, a non-labelled CG3 RNA-based aptamer with 30 bases long for PCA3 is used because it is specific and selective towards PCA3 (Marangoni et al., 2015; Takita et al., 2022, 2023). The operation principle is the opposite of that of redox-labelled aptamers (Nabok et al., 2021; Takita et al., 2023); the presence of redox chemicals $[Fe(CN)6]^{3-/4-}$ redox couple in solution provides efficient charge transfer, which is reduced by conformational changes in aptamers structure upon binding analyte molecules (e. g., PCA3). The impact of various mediums, such as buffer and urine, on the sensitivity and selectivity of the impedimetric biosensors is also examined. Different analytical methods, cyclic voltammetry (CV),

electrochemical impedance spectroscopy (EIS), scanning electron microscopy (SEM), and energy-dispersive X-ray spectroscopy (EDX), were used for sensor characterisation at different stages of its development. The biosensor demonstrated exceptional specificity towards PCA3 and a linear response over various concentrations. The approach significantly reduces the number of tests and reagents required for research.

2. 2- Materials and methods

The schematic diagram in Scheme 1 shows the preparation steps and measurement of the performance of the electrochemical aptasensor for the detection of PCA3. The supplementary materials provide a full description of the materials and methods used in this work.

3. 3- Results and discussion

3.1. Electrochemical characterisations of the fabricated aptasensor

The process of fabricating the PCA3 aptasensor (PCA3/MCH/thiolate aptamer/AuNP/SPCEs) was monitored using CV and EIS measurements. The electrochemical characteristics of the bare electrodes (AuNP/SPCE) were monitored after each step of modification and compared to those of the bare electrodes. The measurements were carried out in a 0.1 M PBS (pH 7.4) solution containing $[Fe\ (CN)_6]^{3-/4-}$ and KCl (5 mM/0.1 M). In this work, $[Fe(CN)_6]^{3-/4-}$ was selected as a redox probe due to its excellent performance compared to other redox probes employed in the label-free EC aptasensor (Capatina et al., 2022). CV is a widely used electrochemical technique for studying electrochemical processes that occur at the interface between an electrode and a solution. In line with theory, the electrode modification changes the peak current observed in the CV curves, which is attributed to the charge transfer resistance (Wang et al., 2021). CV scans were performed on bare electrodes (AuNP/SPCEs) (black curve), after immobilisation of thiolated aptamers (aptamer/AuNP/SPCEs) (red curve), after blocking with MCH (MCH/aptamer/AuNP/SPCEs) (green curve), and after binding 10 nM of PCA3 (PCA3/MCH/aptamer/AuNP/SPCEs) (blue curve), as presented in Fig. 1A. The analysis of these measurements focuses on the different characteristics of $[Fe\ (CN)_6]^{3-/4-}$ by analysing the separation of redox peaks and calculating the ΔEp of the cathodic and anodic waves and the current response. The CV curve demonstrates that the redox probe $[Fe\ (CN)_6]^{3-/4-}$ displayed highly reversible peaks at the bare working electrode of the AuNP/SCPE.

The peak separation (ΔEp) was measured to be 0.212 V and an oxidation current peak of about 106.802 μA as shown in Fig. 1A, black curve. These results are in line with previous studies showing that the addition of gold nanoparticles to the surface of the SPE may significantly enhance the exposed area of AuNPs, leading to improved conductivity of the electrode surface and facilitating electrocatalytic activity and electron transport (Hassani et al., 2020a; Naghshbandi et al., 2023; Wang et al., 2021). As predicted by the immobilisation of thiolate aptamers on the surface of AuNPs/SPCE via Au–S covalent binding (Fig. 1A, red curve), the oxidation peak dropped significantly to 83.7 μA, and ΔEp slightly increased to 0.268V. The likely cause for the decrease in current can be attributed to high resistance at the surface. The electron kinetics at the working electrode surface of AuNPs/SPCE are considerably slower than the rate at which the $[Fe\ (CN)_6]^{3-/4-}$ couple diffuses through the electrolyte solution. As a result, there is a reduction in current and an increase in peak potential (Mushiana et al., 2019). Another factor contributing to this phenomenon is the repulsive steric hindrance caused by the negatively charged phosphate groups of the aptamer. This hindrance repels the negatively charged $[Fe\ (CN)_6]^{3-/4-}$ ion and interferes with the electron transport on the electrode surface, resulting in a peak current reduction (Hassani et al., 2020a; Wang et al., 2021). Adding MCH to the electrode surface, as shown by the green curve in Fig. 1A–is necessary for blocking nonspecific sites that hinder electron transfer. Besides, MCH had a long-chain thiol that helped stabilise aptamer molecules. As a result, an additional barrier forms between the electrode surface and the redox mediator, leading to a drop in the redox peak

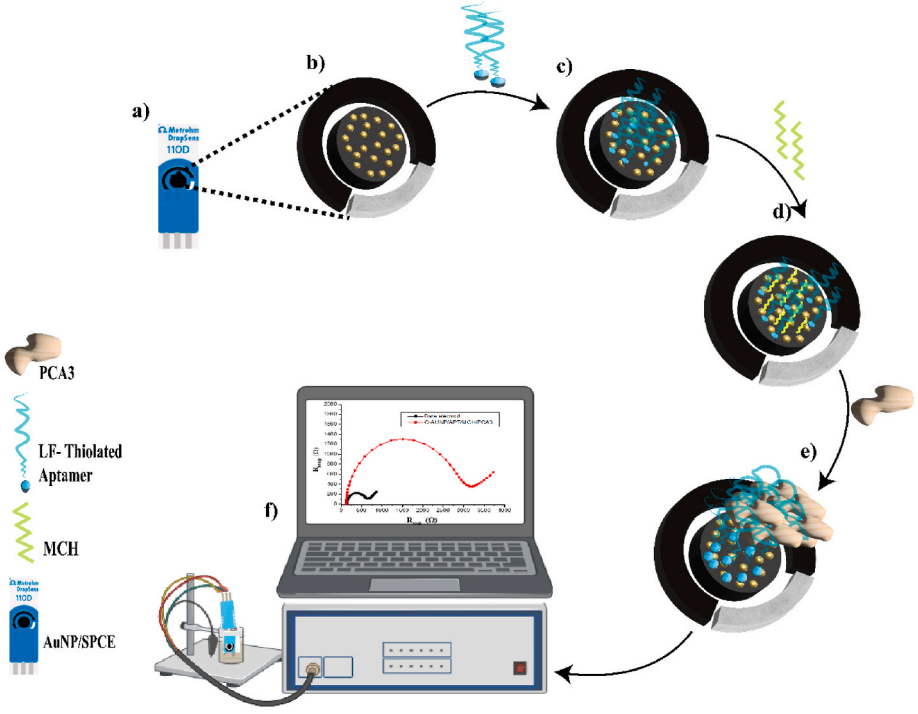

Scheme 1. Schematic diagram of the preparation and performance of the electrochemical aptasensor for detection of PCA3: (a) three-electrode assembly, (b) zoomed-in carbon WE with AuNPs, (c) and (d) WE with immobilised aptamers and MCH, the presence of ferrocene in the solution still enables the charge transfer, (e) binding PCA3 to aptamer caused changes in its configuration and subsequent blocking of charge transfer, (f) three electrochemical set for detection PCA3 with data plotting.

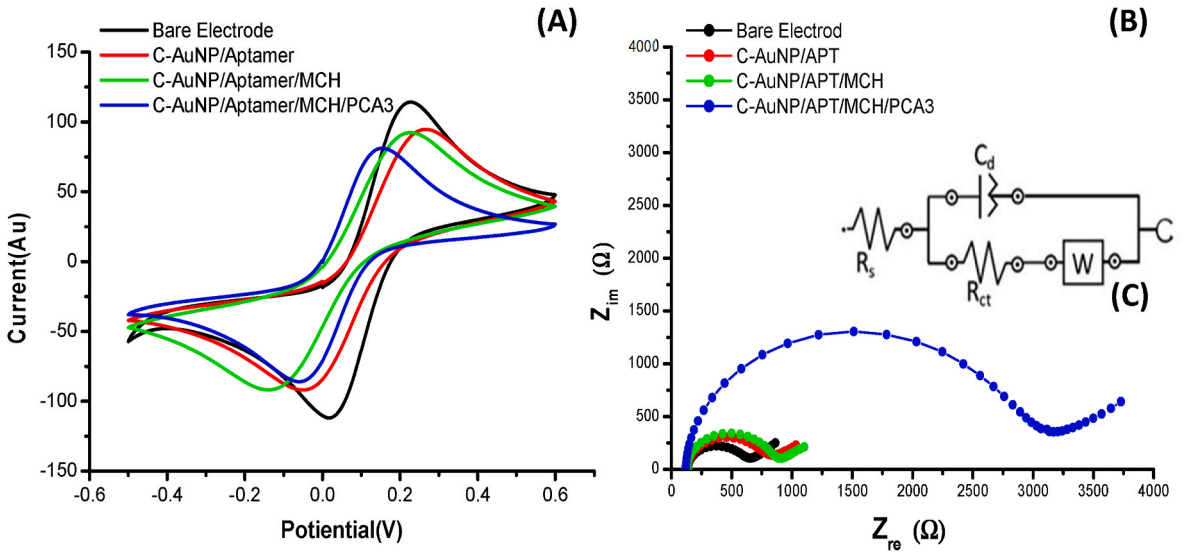

Fig. 1. (**A**) CV curves, (**B**) Nyquist plots of impedance spectra, both data are recorded in 0.1 M PBS (pH = 7.4) containing $[Fe(CN)_6]^{3-/4-}$/KCl (5 mM/0.1 M): on bare Au NPs/SPCE electrodes (black), after immobilisation of thiolate aptamers (red), after blocking gaps with MCH on aptamer/Au NPs/SPCE (green) and after binding PCA3 (10 nM)/MCH/aptamer/AuNPs/SPCE. (**C**) The Randles equivalent circuit was employed to model the electrochemical impedance data (Rs: solution resistance; Cdl: double layer capacitance; R_{CT}: charge transfer resistance; W: Warburg impedance. (For interpretation of the references to colour in this figure legend, the reader is referred to the Web version of this article.)

current to 83.7 μA and a slight increase in the peak-to-peak separation to approximately 0.371 V. Ultimately, it is essential to note that adding 10 nM of PCA3 and its subsequent binding to the aptamer caused conformational changes in the aptamer configuration, which further restricted the electron transport of $[Fe(CN)_6]^{3-/4-}$ ions. As a result, the difference in potential between the peaks raised correspondingly (ΔEp = 0.214 V) in the blue curve in Fig. 1A. Therefore, changes in the electrical resistance of electron transfer occurring during the oxidation/reduction of Fe $[(CN)_6]^{3-/4-}$ at the electrode/solution interface can be considered a detection mechanism and the charge transfer resistance (R_{CT}) can be used as the main detecting parameter. It was proven that the reduction in the peak current may be attributed to the successful hybridisation of PCA3 with CG3-Aptamer. These results are consistent with earlier studies that explained that the immobilised aptamer-target complex formation may interfere with the aptasensor's electrochemical characteristics (Hassani et al., 2020a; Rafiee-Pour et al., 2016).

Subsequently, EIS measurements were conducted on screen-printed electrodes at the same stages of fabrication to validate the voltammetry findings, and the results are shown in Fig. 1B. The EIS spectra provide insights into the electrode and electrolyte interface changes. This information is crucial for understanding the real conditions of aptasensors throughout all fabrication steps, which is needed to produce high-performing responses in electrochemical impedance spectroscopy experiments (Alnaimi et al., 2022; Wang et al., 2021). The impedance spectra are often presented as Nyquist plots where the imaginary part of impedance Z_{im} is plotted against the real part of impedance Z_{re} at different frequencies. The Nyquist plot largely depends on two main parameters: the diameter of the semicircle segment at high-frequency regions correlating to the charge transfer resistance (R_{CT}) at the electrode surface and a linear segment in the low-frequency range corresponding to the diffusion process. In order to get precise quantitative data on the surface changes, the electrochemical impedance data was fitted using the Randles equivalent circuit as a model (Fig. 1C) (Hassani et al., 2020a, 2020b). This representation enables the assessment of the charge-transfer resistance (R_{CT}), which is the main parameter representing electron transfer at the electrode/electrolyte interface. Any modification to the electrode will impact its semi-circular portion (R_{CT}) and the diffusion-limiting process Z_W, which will be determined after each modification step in the EIS measurements. The results of the EIS equivalent modelling are summarised in Table S1 in the supplementary material section. The EIS spectra recorded in a redox electrolyte called ferri-ferrocyanide electrolyte (0.1 M PBS, including 5 mM $[Fe(CN)_6]^{3-/4-}$ in 0.1 M KCl (pH 7.4) at every step of electrode surface modification and presented as Z_{im} vs. Z_{re}, also known as the Nyquist plot in Fig. 1B. The experimental points correspond to frequencies increasing from 0.01 Hz to 100 kHz from right to left. Different curves in Fig. 1B correspond to Nyquist plots of bare electrodes (AuNP/SPCEs) (black curve), electrodes with immobilised thiolated aptamers (aptamer/-AuNP/SPCEs) (red curve), MCH/aptamer/AuNP/SPCEs (green curve), and after binding 10 nM of PCA3 (PCA3/MCH/aptamer/AuNP/SPCEs) (blue curve). Fig. 1B (black curve) shows a small electron transfer resistance of the redox probe R_{CT} = 471.7 Ω, equivalent to the bare SPE impedance (non-immobilised working electrode). It suggests that the gold nanoparticle's presence on the SPCE accelerated the diffusion of $[Fe(CN)_6]^{3-/4-}$ in the bare electrode and increased the reversibility of redox substances on the electrode surface, confirming the CV measurements (Fig. 1B, black curve) (Hassani et al., 2020a; Wang et al., 2021). After immobilisation of aptamers onto the Au NPs/SPCE (Fig. 1B, red curve), the semicircle diameter of the Nyquist plot and respective R_{CT} = 615.8 Ω value increased significantly. The addition of MCH (green curve in Fig. 1B) yields a further increase in R_{CT} to 780 Ω. The higher R_{CT} value indicates that immobilised aptamers and MCH act as a blocking barrier, impeding electron transport between the redox probe and the electrode surface owing to an increase in interface thickness. Furthermore, the negatively charged electrostatic repulsion between the phosphate skeleton aptamer and the negatively charged electrolyte solution $[Fe(CN)_6]^{3-/4-}$ blocked access of the redox probe to the modified electrode surface (Hassani et al., 2020a; Rafiee-Pour et al., 2016; Wang et al., 2021). A significant increase in the R_{CT} value to 2810 Ω (Fig. 1B, blue curve) was seen upon interaction with 10 nM PCA3 and the aptamer and subsequent changes in the aptamer configuration and the aptamer. As previously indicated, the aptamer-PCA3 complex's significant steric hindrance effect increased the electrode surface's spatial site resistance and hindered the electron transfer rate (Hassani et al., 2020a, 2020b). These results obtained via EIS were consistent with those obtained in the CV data, where a decrease in peak current was also observed when aptamer, MCH, and PCA3 were adsorbed on the electrode's surface to block nonspecific sites, revealing that the modifying layers were

successfully immobilised onto the electrode's surface. The supplementary information fully describes electrode surface morphology studies using FE-SEM and EDX.

3.2. Analytical performance for the electrochemical aptasensor: PCA3 detection in buffer

This study presents the development of a label-free aptasensor for determining PCA3. The detection is based on a specific binding interaction between the CG3 aptamer and PCA3, which forms a PCA3/CG3-APT complex. This complex hinders electron transfer and results in an increase in charge transfer resistance (R_{CT}) between the solution-based redox probe $[Fe(CN)_6]^{3-/4-}$ and the electrode surface. In this study, we investigate the connection between the change of R_{CT} and the PCA3 level, i.e., the change of R_{CT} is positively related to the PCA3 level, so EIS can quantitatively test the determination of PCA3. Initially, the fabricated aptasensors were incubated in a 0.01 M PBS solution with a pH of 7.5, containing different concentrations of PCA3 ranging from 10 nM to 0.1 pM.

Afterwards, the aptasensor was thoroughly rinsed with a washing buffer to remove unbound PCA3. Following the incubation period, the EIS tests were performed by immersing the aptasensor into a solution containing 5 mM $[Fe(CN)_6]^{3-/4-}$ and 0.1 M KCl at a pH of 7.4. The Nyquist plots representing the specific binding interaction between PCA3 and the aptasensor were measured and shown in Fig. 2A. The impedance spectra obtained were analysed using the modified Randles' equivalent circuit, as shown in Fig. 1, inset C. Fig. 2A clearly demonstrates that the aptamer sensor's R_{CT} is the lowest in the blank solution. As the concentration of PCA3 rises, the impedance value increases gradually, indicating a specific binding interaction between the CG3-aptamer and PCA3. Fig. 2B demonstrates a strong linear correlation between the electrochemical aptamer sensor and PCA3 within the 1 nM −10 pM concentration range with a low detection limit of 1 fM. The linear regression equation used was Y (R_{CT}) = *428.08* Log *(C PCA3 nM)* + *6336.8,* and the correlation coefficient was found to be (R^2 = 0.91). The carbon-gold nanoplatforms can be attributed to the lower detection limit due to their bio-functionalization compatibility and electrocatalytic abilities. This finding is consistent with previously published research (Harahsheh et al., 2021; Makableh et al., 2023; Wang et al., 2021). Moreover, compared to earlier techniques for PCA3 detection, as shown in Table 1, our study's detection limit shows promise for low concentration PCA3 without complicated modification steps. This simple, quick, and low-cost approach is suggested as a promising label-free aptasensor using EIS, indicating its potential for PCA3 detection. Furthermore, the reproducibility of the developed aptasensor has been evaluated by determining a 10 nM PCA3 solution with four independent aptasensors made using the same procedure (Fig.S2). For evaluation of the repeatability of the aptasensor, the same fabricated aptasensor was used to measure PCA3 (10 nM) three times. The relative standard deviation (RSD) for reproducibility was 7.31%, and for repeatability, it was 3.89%. The developed aptasensor has good reproducibility and repeatability in the detection of PCA3.

3.3. Selectivity study of the label-free electrochemical aptasensor

Selectivity is vital in biosensing platforms; the capacity to detect and quantify a target analyte properly in real samples such as urine or serum is also regarded as a significant analytical characteristic that influences the aptasensor's efficacy in clinical analysis. In this regard, the selectivity of the developed label-free aptasensor was evaluated by taking the change in R_{CT} before and after exposure to the analyte ($\Delta R_{CT} = R_{CT}$ (after)- R_{CT} (before)) as the evaluating indicator. Under similar conditions for experiments, 10 nM concentrations of prostate-specific antigen (PSA), bovine serum albumin (BSA), and a non-complementary PCA3 were produced as interfering compounds. Since PSA and BSA are the most prevalent proteins in the body in physiological settings, they were chosen as possible interferents. Fig. 3 shows that the EIS response (ΔR_{CT}) to the target analyte PCA3 is significantly larger than responses to all three selected interferants at the same concentration level having values of ΔR_{CT} similar to the background level (e.g., the response in the absence of the target analyte). These findings proved the high specificity of the developed PCA3 electrochemical aptasensor, making it a potential candidate for practical applications. The exceptional selectivity of this sensor is related to the extremely specific binding interaction of the CG3 aptamer with the PCA3 target, as was shown earlier in our previous research (Takita et al., 2021, 2023).

3.4. Detection of PCA3 in artificial urine

Although our aptasensor demonstrated excellent sensitivity and selectivity for PCA3, it is important to evaluate the feasibility of its performance in more complex samples. For this purpose, a range of PCA3 concentrations, varying from 10 to 0.1 pM, were added to artificial urine solutions containing (simulating human urine) and evaluated under the conditions described earlier in Section S1.2 in the supplementary file. As shown in Fig. 4A, the EIS measurements in urine yield a

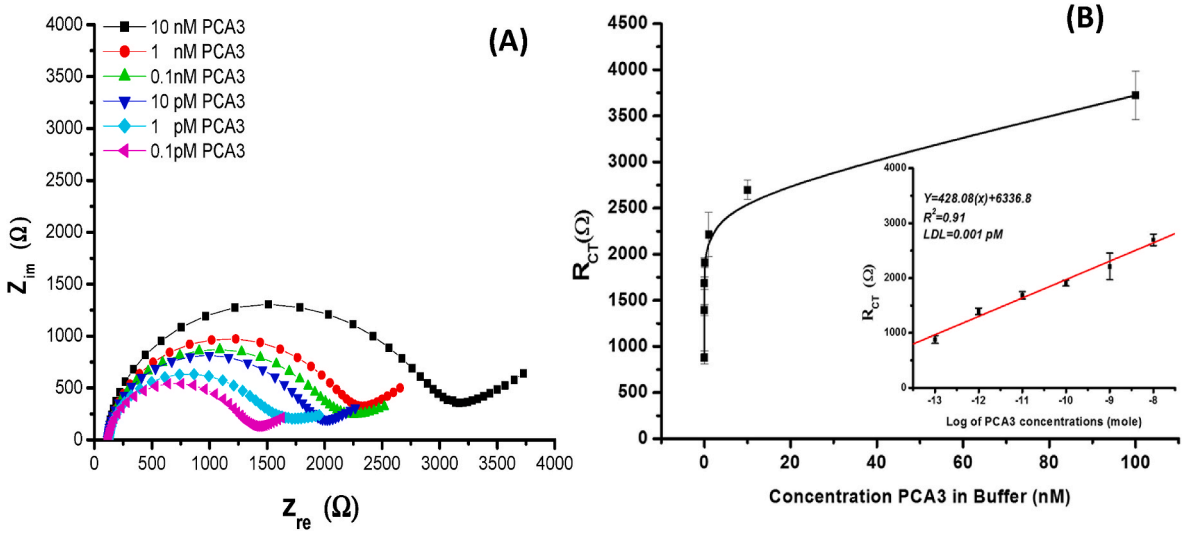

Fig. 2. (A) EIS of the proposed aptasensor PCA3 range from 10 to 0.1pM in 5 mM $[Fe(CN)6]^{3-/4-}$0.1 M PBS (pH 7.0) $^{-1}$ M KCl, **(B)** Plots of R_{CT} vs PCA3 concentration with a correlation coefficient of 0.91.

Table 1
Comparison of this aptasensor with other methods previously reported for PCA3 detection.

DETECTION METHOD	Detection Limit	Biorecognition Element	Biosensor Configuration	Ref.
ELECTROCHEMICAL (EIS)	0.128 nmol/L	genosensor	Chitosan and carbon nanotubes	Soares et al. (2019)
ELECTROCHEMICAL (VOLTAMMETRY AND EIS)	0.04 ng/mL	aptasensor	Au/SPE and ID-Au electrode	Nabok et al. (2021)
OPTICAL (TIRE)	1 pM	aptasensor	Au coated Glass	Takita et al. (2021)
OPTICAL (SERS)	3 fM	genosensor	Au -SERS platform	Fu et al. (2019)
Electrochemical multiplex detection (chronoamperometric)	4.4 pM	genosensor	Different screen-printed electrochemical cells (SPECs)	Sánchez-Salcedo et al. (2021)
RT-PCR	1.25 copies/ μL	aptasensor	PCR Plate	Vaananen et al. (2008)
ELECTROCHEMICAL (EIS)	0.001 pM	aptasensor	AuNPs modified SPCE	In This work

Where is TIRE: Total Internal Reflection Ellipsometry; **SERS:** Surface Enhancement Raman Spectroscopy; **ID-Au:** Gold Interdigitated Electrode.

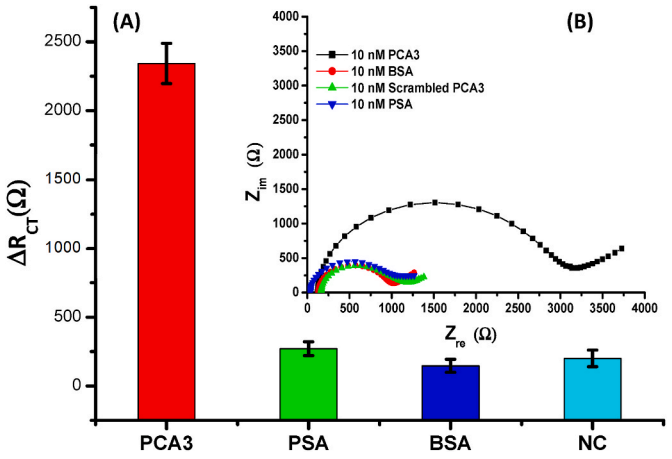

Fig. 3. (A)The suggested aptasensor's specificity for 10 nM PCA3 was evaluated by (B) comparing its EIS signals to 10 nM of interfering substances such as PSA, BSA, and scrambled PCA3. The error bars indicate the standard deviations of three sets of experiments.

linear correlation in a wide range of PCA3 concentrations of 0.1 pM–1 nM. The detection limit was estimated to be 0.023 pM using the regression equation $Y(R_{CT}) = 507.5 \text{ Log } (C \text{ PCA3 nM}) + 6922.7$, and the correlation coefficient was found to be ($R^2 = 0.95$) presented in Fig. 4B. Notably, the sensitivity is still reasonably good, though slightly lower than that in buffer solution, owing to the presence of other proteins in the synthetic urine, causing interference but still giving lower detectable linearity.

4. Conclusion

Significant progress has been made in developing an electrochemical atpasensor for detecting the prostate cancer marker PCA3. The process involved a combination of the power of an electrochemical detection technique (EIS) with signal amplification, good conductivity from nanotechnology carbon screen-printed electrodes functionalised with gold nanoparticles (C–AuNP), and the benefits of an aptamer-based approach rather than an antibody (unlabelled CG3 RNA-based aptamer) as a bioreceptor, giving a screening alternative for prostate cancer. The aptasensor demonstrated remarkably high sensitivity for PCA3 detection in different mediums, buffer, and artificial urine, with a detection limit of 1 fM and 20 fM, respectively. Negative control tests showed high selectivity for the electrochemical aptasensor. The developed electrochemical aptasensor could be suitable for early and point-of-care prostate cancer diagnostics. Additional research is necessary to investigate aptasensor stability and analyse real urine samples from prostate cancer patients. Simultaneous detection of several prostate cancer biomarkers could also be beneficial.

Funding

This project did not receive any specific grant from public, commercial, or not-for-profit funding agencies.

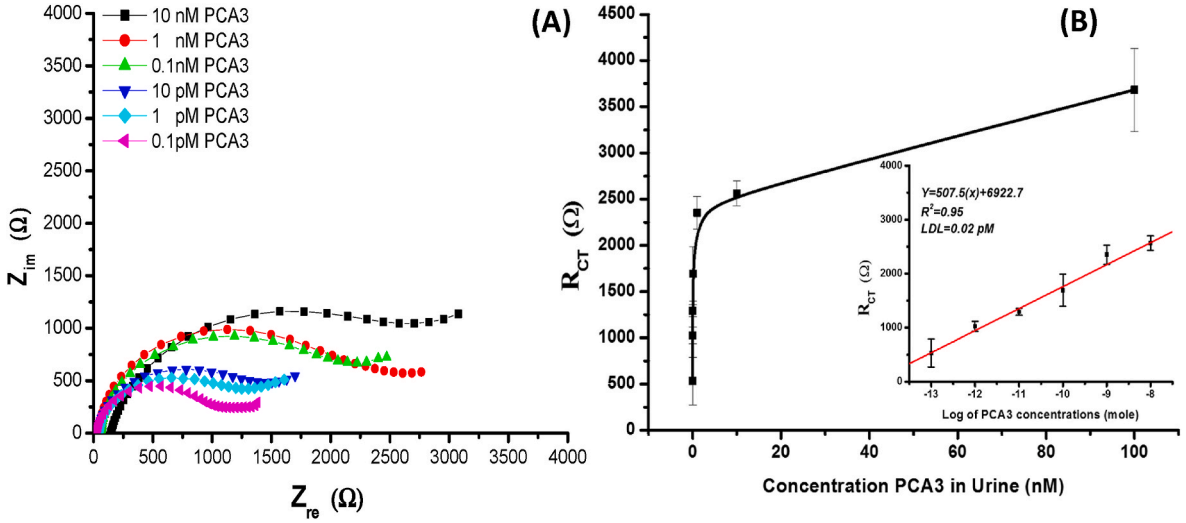

Fig. 4. **(A)** EIS of the proposed aptasensor in artificial urine PCA3 ranging from 10 to 0.1pM in 5 mM $[Fe(CN)6]^{3-/4-}$0.1 M PBS (pH 7.0) $^{-1}$ M KCl, **(B)** Plots of R_{CT} vs PCA3 concentration with a correlation coefficient of 0.95.

CRediT authorship contribution statement

Sarra Takita: Writing – review & editing, Writing – original draft, Methodology, Investigation, Formal analysis, Data curation. **Alexi Nabok:** Writing – review & editing, Supervision, Project administration, Methodology, Conceptualization. **Magdi Mussa:** Writing – review & editing, Validation, Formal analysis. **Matthew Kitchen:** Resources, Formal analysis. **Anna Lishchuk:** Writing – review & editing, Supervision. **David Smith:** Writing – review & editing, Supervision, Resources, Methodology.

Declaration of competing interest

The authors declare that they do not own any identifiable conflicting financial or personal interests or relationships that might have potentially influenced the findings presented in this study.

Data availability

All the data underlying the results is available as part of the article and supplementary sheet. The raw data are not publicly available, as this raw data will be used in other future contributions

Appendix A. Supplementary data

Supplementary data to this article can be found online at https://doi.org/10.1016/j.biosx.2024.100462.

References

Adabi, Mohsen, Esnaashari, S.S., Adabi, Mahdi, 2021. J. Porous Mater. 28, 415–421.
Adhyam, M., Gupta, A.K., 2012. Indian J. Surg. Oncol. 3, 120–129.
Alnaimi, A., Al-Hamry, A., Makableh, Y., Adiraju, A., Kanoun, O., 2022. Biosensors 12, 1130.
Bernardeau, S., Charles, T., Fromont-Hankard, G., Irani, J., 2017. Prog. Urol. 27, 325–330.
Bourdoumis, A., Papatsoris, A.G., Chrisofos, M., Efstathiou, E., Skolarikos, A., Deliveliotis, C., 2010. Int. Braz J. Urol. 36, 665–669.
Capatina, D., Lupoi, T., Feier, B., Blidar, A., Hosu, O., Tertis, M., Olah, D., Cristea, C., Oprean, R., 2022. Biosensors 12, 440.
Center, M.M., Jemal, A., Lortet-Tieulent, J., Ward, E., Ferlay, J., Brawley, O., Bray, F., 2012. Eur. Urol. 61, 1079–1092.
Das, J., Kelley, S.O., 2020. Angew. Chem. Int. Ed. 59, 2554–2564.
Drobysh, M., Liustrovaite, V., Baradoke, A., Rucinskiene, A., Ramanaviciene, A., Ratautaite, V., Viter, R., Chen, C.-F., Plikusiene, I., Samukaite-Bubniene, U., Slibinskas, R., Ciplys, E., Simanavicius, M., Zvirbliene, A., Kucinskaite-Kodze, I., Ramanavicius, A., 2022a. Int. J. Mol. Sci. 23, 6768.
Drobysh, M., Liustrovaite, V., Baradoke, A., Viter, R., Chen, C.-F., Ramanavicius, A., Ramanaviciene, A., 2022. Biosensors 12, 593.
Drobysh, M., Liustrovaite, V., Kanetski, Y., Brasiunas, B., Zvirbliene, A., Rimkute, A., Gudas, D., Kucinskaite-Kodze, I., Simanavicius, M., Ramanavicius, S., Slibinskas, R., Ciplys, E., Plikusiene, I., Ramanavicius, A., 2024. Sci. Total Environ. 908, 168154.
Fang, B.-Y., Wang, C.-Y., Li, C., Wang, H.-B., Zhao, Y.-D., 2017. Sens. Actuators, B 244, 928–933.
Forouzanfar, S., Alam, F., Pala, N., Wang, C., 2020. J. Electrochem. Soc. 167, 067511.
Fu, X., Wen, J., Li, J., Lin, H., Liu, Y., Zhuang, X., Tian, C., Chen, L., 2019. Nanoscale 11, 15530–15536.
Groskopf, J., Aubin, S.M., Deras, I.L., Blase, A., Bodrug, S., Clark, C., Brentano, S., Mathis, J., Pham, J., Meyer, T., Cass, M., Hodge, P., Macairan, M.L., Marks, L.S., Rittenhouse, H., 2006. Clin. Chem. 52, 1089–1095.
Harahsheh, T., Makableh, Y.F., Rawashdeh, I., Al-Fandi, M., 2021. Biomed. Microdevices 23, 46.
Hassani, S., Rezaei Akmal, M., Salek Maghsoudi, A., Rahmani, S., Vakhshiteh, F., Norouzi, P., Ganjali, M.R., Abdollahi, M., 2020a. Front. Bioeng. Biotechnol. 8.
Hassani, S., Salek Maghsoudi, A., Rezaei Akmal, M., Rahmani, S.R., Sarihi, P., Ganjali, M. R., Norouzi, P., Abdollahi, M., 2020b. J. Pharm. Pharmaceut. Sci. 23, 243–258.
Hessels, D., Schalken, J.A., 2009. Nat. Rev. Urol. 6, 255–261.
Jolly, P., Formisano, N., Estrela, P., 2015. Chem. Pap. 69.
Kanyong, P., Rawlinson, S., Davis, J., 2016. J. Cancer 7, 523–531.
Karapetis, S., Nikolelis, D., Hianik, T., 2018. Sensors 18, 4218.
De Kok, J.B., Verhaegh, G.W., Roelofs, R.W., Hessels, D., Kiemeney, L.A., Aalders, T.W., Swinkels, D.W., Schalken, J.A., 2002. Cancer Res. 62, 2695–2698.
Kupelian, P.A., Mahadevan, A., Reddy, C.A., Reuther, A.M., Klein, E.A., 2006. Urology 68, 593–598.
Li, W., Yang, Y., Ma, C., Song, Y., Qiao, X., Hong, C., 2020. Sens. Actuators, B 324, 128772.
Lomas, D.J., Ahmed, H.U., 2020. Nat. Rev. Clin. Oncol. 17, 372–381.
Ludwig, J.A., Weinstein, J.N., 2005. Nat. Rev. Cancer 5, 845–856.
Macefield, R.C., Metcalfe, C., Lane, J.A., Donovan, J.L., Avery, K.N.L., Blazeby, J.M., Down, L., Neal, D.E., Hamdy, F.C., Vedhara, K., 2010. Br. J. Cancer 102, 1335–1340.
Makableh, Y., Athamneh, T., Ajlouni, M., Hijazi, S., Alnaimi, A., 2023. Sensors and Actuators Reports 5, 100158.
Marangoni, K., Neves, A.F., Rocha, R.M., Faria, P.R., Alves, P.T., Souza, A.G., Fujimura, P.T., Santos, F.A.A., Araújo, T.G., Ward, L.S., Goulart, L.R., 2015. Sci. Rep. 5, 12090.
Mitchell, P.S., Parkin, R.K., Kroh, E.M., Fritz, B.R., Wyman, S.K., Pogosova-Agadjanyan, E.L., Peterson, A., Noteboom, J., O'Briant, K.C., Allen, A., Lin, D.W., Urban, N., Drescher, C.W., Knudsen, B.S., Stirewalt, D.L., Gentleman, R., Vessella, R. L., Nelson, P.S., Martin, D.B., Tewari, M., 2008. Proc. Natl. Acad. Sci. USA 105, 10513–10518.
Montagut, E.J., Vilaplana, L., Martin-Gomez, M.T., Marco, M.P., 2020. ACS Infect. Dis. 6, 3237–3246.
Moyer, V.A., 2012. Ann. Intern. Med. 157, 120.
Mushiana, T., Mabuba, N., Idris, A.O., Peleyeju, G.M., Orimolade, B.O., Nkosi, D., Ajayi, R.F., Arotiba, O.A., 2019. Sens. Bio-Sensing Res. 24, 100280.
Mussa, M., Shtawa, A., Takita, S., 2023. Eng Proc 56, 98.
Mussa, M.H., Zahoor, F.D., Lewis, O., Farmilo, N., 2021. Eng. Proc. 11, 9.
Nabok, A., Abu-Ali, H., Takita, S., Smith, D.P., 2021. Chemosensors 9, 59.
Naghshbandi, B., Adabi, M., Pooshang Bagheri, K., Tavakolipour, H., 2023. J. Nanobiotechnol. 20, 534.
Pasinszki, T., Krebsz, M., Tung, T.T., Losic, D., 2017. Sensors 17, 1919.
Pfeiffer, F., Mayer, G., 2016. Front. Chem. 4.
Ploussard, G., de la Taille, A., 2018. Expert Rev. Anticancer Ther. 18, 1013–1020.
Rafiee-Pour, H.-A., Behpour, M., Keshavarz, M., 2016. Biosens. Bioelectron. 77, 202–207.
Rizwan, M., Elma, S., Lim, S.A., Ahmed, M.U., 2018. Biosens. Bioelectron. 107, 211–217.
Rodrigues, V.C., Soares, J.C., Soares, A.C., Braz, D.C., Melendez, M.E., Ribas, L.C., Scabini, L.F.S., Bruno, O.M., Carvalho, A.L., Reis, R.M., Sanfelice, R.C., Oliveira, O. N., 2021. Talanta 222, 1–10.
Sánchez-Salcedo, R., Miranda-Castro, R., De-los-Santos-Álvarez, N., Lobo-Castañón, M.J., 2021. Biosens. Bioelectron. 192, 113520.
Sartori, D.A., Chan, D.W., 2014. Curr. Opin. Oncol. 26, 259–264.
Shayesteh, O.H., Ghavami, R., 2020. Spectrochim. Acta Part A Mol. Biomol. Spectrosc. 226, 117644.
Soares, J.C., Soares, A.C., Rodrigues, V.C., Melendez, M.E., Santos, A.C., Faria, E.F., Reis, R.M., Carvalho, A.L., Oliveira, O.N., 2019. ACS Appl. Mater. Interfaces 11, 46645–46650.
Sung, H., Ferlay, J., Siegel, R.L., Laversanne, M., Soerjomataram, I., Jemal, A., Bray, F., 2021. CA. Cancer J. Clin. 71, 209–249.
Takita, S., Nabok, A., Lishchuk, A., Mussa, M.H., Smith, D., 2022. Eng. Proc. 16, 6.
Takita, S., Nabok, A., Lishchuk, A., Mussa, M.H., Smith, D., 2023. Eng 4, 367–379.
Takita, S., Nabok, A., Lishchuk, A., Smith, D., 2021. Int. J. Mol. Sci. 22, 12701.
Tinzl, M., Marberger, M., Horvath, S., Chypre, C., 2004. Eur. Urol. 46, 182–187.
Toh, S.Y., Citartan, M., Gopinath, S.C.B., Tang, T.-H., 2015. Biosens. Bioelectron. 64, 392–403.
U.S National Cancer Institute, 2017. SEER Cancer Statistics Review (CSR) 1975-2016 [WWW Document]. U.S. Dep. Heal. Hum. Serv. URL. https://seer.cancer.gov/archive/csr/1975_2016/index.html#contents.
Vaananen, R.-M., Rissanen, M., Kauko, O., Junnila, S., Väisänen, V., Nurmi, J., Alanen, K., Nurmi, M., Pettersson, K., 2008. Clin. Biochem. 41, 103–108.
Velonas, V., Woo, H., Remedios, C., Assinder, S., 2013. Int. J. Mol. Sci. 14, 11034–11060.
Wang, X., Su, J., Zeng, D., Liu, G., Liu, L., Xu, Y., Wang, C., Liu, X., Wang, L., Mi, X., 2019. Talanta 201, 119–125.
Wang, Y., Chen, L., Xuan, T., Wang, J., Wang, X., 2021. Front. Chem. 9.
Wu, A.K., Reese, A.C., Cooperberg, M.R., Sadetsky, N., Shinohara, K., 2012. Prostate Cancer Prostatic Dis. 15, 100–105.